ARTICLE

Journal of Applied Polymer SCIENCE   WILEY

Time and volume-ratio effect on reusable polybenzoxazole nanofiber oil sorption capacity investigated via machine learning

Kamil Oflaz[1] 🄳 | Zarina Oflaz[2] 🄳 | Ilkay Ozaytekin[1] 🄳 | Kevser Dincer[3] | Rabia Barstugan[1]

[1]Department of Chemical Engineering, Faculty of Engineering and Natural Sciences, Konya Technical University, Konya, Turkey

[2]Department of Insurance and Social Security, Faculty of Economics and Administrative Sciences, KTO Karatay University, Konya, Turkey

[3]Department of Mechanical Engineering, Faculty of Engineering and Natural Sciences, Konya Technical University, Konya, Turkey

Correspondence
Kamil Oflaz, Department of Chemical Engineering, Faculty of Engineering and Natural Sciences, Konya Technical University, Konya, Turkey.
Email: kamiloflazz@gmail.com

Abstract

Diesel oil sorption capacities (DOSCs) of polybenzoxazole/polyvinylidene fluoride nanofiber mats with four different groups (-O-, -S-S-, phenylene and diphenylene) in the main chain structures were investigated. Different experimental duration and diesel-oil/tap-water volume ratio pairs were used for diesel oil sorption. No degradation was observed in the nanofiber mat structures after diesel oil sorption. The characterizations of polybenzoxazole (PBO) nanofibers with high diesel oil selectivity were performed by scanning electron microscopy, atomic force microscopy, Fourier transform infrared spectroscopy, x-ray diffraction, thermal gravimetric analysis, differential scanning calorimetry, Brunauer–Emmett–Teller (BET), and contact angle measurement analysis. According to the result of characterizations, superoleophilic and superhydrophobic nanofiber mats show high water contact angle value in the range of 132–140° and show high separation efficiency. In this study, we integrated ensemble gradient boosting model (XGBoost) to predict the DOSC of sorbent nanofiber and obtain an optimal set of conditions to maximize the DOSC. The predicted PBO-E sorbent at the 0.5 ratio of diesel-oil/tap-water measured at the end of the 3rd minute showed the most reliable and stable diesel oil sorption with at least 9.39 and at most 12.33 g/g sorbent with 95% of confidence.

KEYWORDS

electrospinning, fibers, machine learning, nanoparticles, nanowires, and nanocrystals, oil and gas, XGBoost

1 | INTRODUCTION

With the rapid growth of the maritime industry worldwide, oily wastewater caused by marine collisions that occur during transport and storage, mining in the oil industry and shipping waste poses a significant environmental and safety issue.[1–8] Petroleum wastes include volatile organic compounds, polycyclic aromatic hydrocarbons, and other toxic–harmful substances.[9,10] Additionally, petroleum wastewater emissions are typically highly persistent and substantially damage the marine environment and all the living species.[11–13]

Resolving the contamination problem associated with industrial diesel oil and other oil wastewaters has become a topic of high priority in recent years. The physical and chemical methods widely used in the treatment of petroleum wastewater include coagulation, electrochemical coagulation, and membrane technologies.[14] However, the high costs of these methods limit their applicability.[15,16]

To overcome this global environmental threat, scientists are actively researching new and successful materials to extract oil/water mixtures and effectively recycle oil from wastewater. Mixed oils in water can be extracted using the absorption method. Natural sorbents including zeolites, fabrics, cotton, and linen, which have broad surface area and high porosity, are typically used because of their inexpensive application for diesel oil sorption.[17-22] However, the practical application of these sorbents is limited because of their low separation efficiency, low absorption capacity, and no reuse. The fabrication of functionalized materials, therefore, becomes important for the treatment of oil-contaminated water. In recent studies in this field, materials with high hydrophobic properties, such as PDMS coated superhydrophilic copper mesh,[23] amino carbon nanotube modified reduced graphene oxide aerogel,[24] nanocellulose-based composite materials that can be used in wastewater treatment as bio-based sorbents or precipitants[25] and encapsulation of camelina oil extract by tannic acid[26] have been studied in wastewater treatment and reuse. Materials with super-hydrophobic and self-cleaning properties, also known as the "lotus effect", and low surface energy are significant in this regard.[27-30] It is also essential to ensure that the sorbent materials do not degrade and are highly selective.

Studies on sorption materials used in wastewater are mostly preferred to be environmentally friendly and deterioration-resistant against pollutants. Studies are carried out not only on diesel oil but also on semiconductor or composite materials with high sorption capacity for dyes, one of the biggest contaminants in industrial wastewater.[31-34] PBOs are also semi-conductive materials. However, it varies depending on the chain length and chain structure, the electrical conductivity of PBOs is around 10^{-8} S/cm. The load distribution resulting from the conjugated structure of PBOs allows these materials to be used in other contaminants in the water.

Aromatic heterocyclic polymers of PBO have been studied since the early 1980s. Their π-conjugated and rigid structure brings many outstanding optical properties as well as mechanical properties and thermal stability.[35-37] Therefore, recently, many conjugated PBOs have been synthesized and the optical and electronic properties have been investigated in detail.[38,39] PBOs were generally used in gas adsorption isotherm studies in sorption studies. Some of these studies; CO_2, N_2, and CH_4 comparative adsorption isotherm study of microporous PBOs,[40] gas and vapor sorption study with triptycene-based PBOs.[41] Along with PBO, it is found that perfluoropolymers also have N_2/CH_4 gas separation properties.[42] Studies on the oil separation feature of the PBOs have not been found. To our best knowledge, PBO mats were used for the first time in oil separation in this study.

Electrospinning is one of the most common methods for the fabrication of nanofiber. The electrospin method is based on the formation of nano-sized fibers from the electrospin solution under the effect of electric field forces. Nanofibers produced by electrospin method contribute to the development of high performance products in air filter application,[43] electrically conductive materials,[44] electrocatalysts,[45] encapsulation,[46] energy applications,[47-49] and oil separation[50] applications due to their superior properties such as low density, high porosity, interconnected pore structure with high permeability, small fiber diameter and high surface area properties. Recently, for oil/water separation, electrospun flexible nanofibrous materials with superwetting properties have received enormous amounts of interest. Hydrophobic materials such as poly(vinylidene fluoride) (PVDF) have generally been used extensively to develop electrospinning membranes for the separation of oil/water, and it is claimed that this process demonstrates high efficiency of separation.[51,52]

In this study, electrospun PBO nanofiber materials with high resistance to chemical solvents, diesel oil, and tap water were used. Super oil absorption and water repellent properties of these hydrophobic nanofiber mats were utilized. Diesel oil sorption capacity (DOSC) values were obtained as experimental data. No degradation was observed in the nanofiber mats after sorption, thereby allowing our mats to be reusable.

Since the replication of the experiments are costly and time consuming, the experimental data is limited in terms of size and include not repeated independent experiments. A key strategy for deeper understanding of the nature behind the limited experimental data is the integration of computational methods. Moreover, the incorporation of computational tools might reduce the expenses spent on experiments and also save time. In this study, we performed statistical analysis and applied machine learning models to effectively evaluate the results of the experiments conducted and to study the experimental conditions€™ effects on DOSC.

Few studies explored oil sorption by using statistical models, particularly the response surface design model[53-55] and regression model.[56] In recent studies IF-THEN rules in fuzzy models have been applied extensively to analyze adsorption[57] and removal efficiency[58,59] in nanocomposite studies. However, fuzzy IF-THEN rules model requires each feature in data set to follow a normal distribution or it is needed to establish particular antecedent fuzzy set for each variable.[60] Thus, the procedure is time-consuming and difficult to use in application.

In contrast, ensemble machine learning models do not have a parametric assumption and do not require additional transformation of the data set. Moreover, the ensemble model is applicable both for numerical and

categorical inputs and outputs. Ensemble learning is a powerful predictive method that combines several models by bagging or boosting algorithms. That is, ensemble methods can achieve greater precision than a single learning algorithm. Moreover, ensemble models provide global feature selection, thereby decreasing the bias and variance of the predicted values, and overcome the over-fitting problems encountered by a single model resulting in a poor prediction performance.[61]

In this study, we integrated tree-based ensemble models, namely, random forest (RF) and extreme gradient boosting (XGBoost), to predict the DOSC of sorbent nanofiber and obtain an optimal set of conditions to maximize the DOSC. The models were implemented on a train set and validated on a test set. The root mean square error (RMSE), mean absolute percentage error (MAPE), and mean absolute error (MAE) metrics were used to evaluate the prediction performances of the models and select the most accurate predictive model. Moreover, we used Shapley Additive Explanations (SHAP) values proposed by Lundberg and Lee[62] to interpret the model. To our best knowledge, it is a first study investigating oil sorption capacity by ensemble machine learning model.

We hope that our study is consistent with the current water treatment technologies, and that it will play a complementary role in this area.

2 | MATERIALS AND METHODS

2.1 | Materials

In this study, four different PBO with different groups (containing -O-, -S-S-, phenylene and diphenylene) in the main chains obtained by Özaytekin et al.[63–65] were used. The structural formulas for the four different PBOs are shown in Figure 1. N, N-Dimethylformamide (DMF; Sigma-Aldrich) and acetone (Carlo Erba) were used as solvents to prepare mats via electrospinning. Additionally, for PBO mats, the poly(vinylidene fluoride-co-hexafluoropropylene) (PVDF; Sigma-Aldrich) hybrid polymer was preferred. Five different solutions were prepared for the electrospinning process. The first of these solutions was prepared with PVDF (0.1 g), DMF (0.7 ml), acetone (0.3 ml), and 0.3% graphene. The remaining four solutions were prepared with PVDF (0.1 g), DMF (0.7 ml), acetone (0.3 ml), PBO (0.001 g), and 0.3% graphene. The electrospinning technique was performed with a voltage, distance, and flow rate of 16 kV, 15 cm, and 0.4 ml/h, respectively.[66] The production of PBO nanofiber mats is given in Figure 2 as a scheme. The contents of the nanofiber mats and their codes are presented in Table 1.
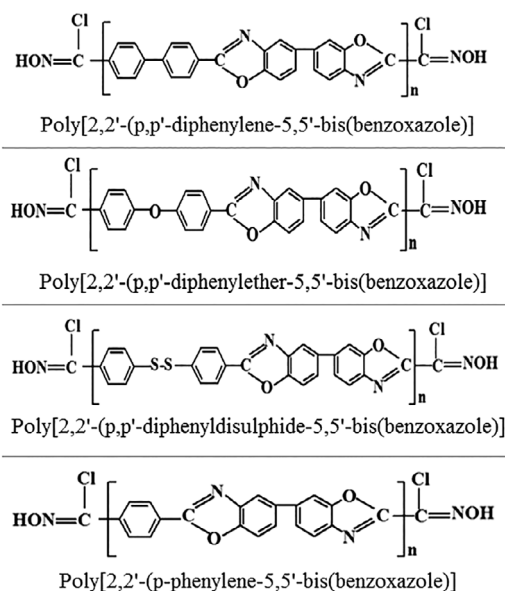

FIGURE 1   The formulas of PBOs

2.2 | Sorption capacity experiment

In this study, we aimed to determine the DOSC for P and PBO doped nanofiber mats. The experiment was performed at room temperature ($\pm$ 25°C). First, dry nanofiber mats were weighed on an analytical balance, and their m_0 values were determined. Four diesel-oil/tap-water mixtures were prepared in diesel-oil/tap-water volume ratios of 0.25, 0.5, and 0.75 in 5 ml to the beakers (Figure 3). The increase in the mass of nanofiber mats at the 1st, 2nd, 3rd, and 4th minutes in mixtures was reported by weighting with an analytical balance. The time was recorded using a digital clock. After the 1st, 2nd, 3rd, and 4th minutes, the wet nanofiber sorbent was removed from the mixture by using forceps, and the mass of the sorbent was measured after 2 min of drainage. The DOSC values of the nanofiber mats were determined by Equation 1[67] as follows:

$$q = \left[m_{nf} - (m_0 + m_w)\right]/m_0, \tag{1}$$

where q denotes the DOSC (g/g sorbent), m_{nf} the mass of the sorbent after 2 min of drainage (g), m_0 the initial mass of the sorbent nanofibers (g), and m_w the mass of the sorbent nanofiber after tap water sorption (g).

2.3 | Characterization

The characterizations of the PBO nanofiber mats provided in the previous study[66] are given as follows: "SEM analysis
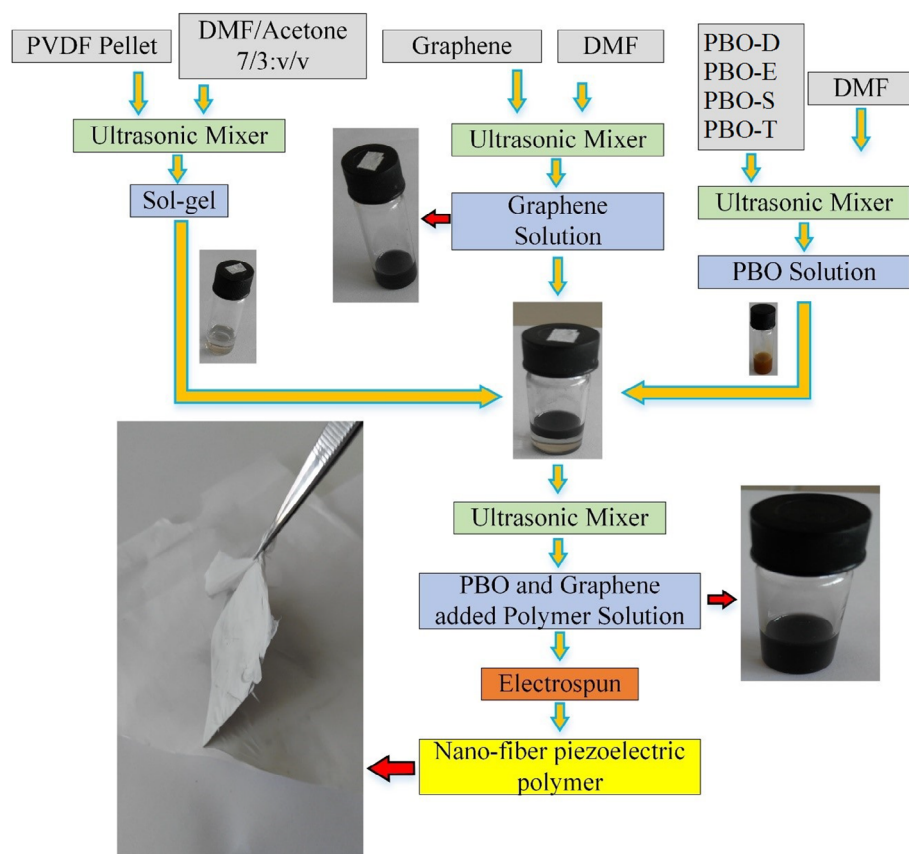
FIGURE 2 The scheme of PBO nanofiber mats production[66] [Color figure can be viewed at wileyonlinelibrary.com]

TABLE 1 The content of the nanofiber mats and their codes

Fiber mat content	Fiber mat code
PVDF	P
PVDF+Poly[2,2′-(p,p'-diphenylene-5,5′-bis (benzoxazole)] + Graphene	PBO-D
PVDF+Poly[2,2′-(p,p'-diphenylether-5,5′-bis (benzoxazole)] + Graphene	PBO-E
PVDF+Poly[2,2′-(p,p'-diphenyldisulphide-5,5′-bis(benzoxazole)] + Graphene	PBO-S
PVDF+Poly[2,2′-(p-phenylene-5,5′-bis (benzoxazole)] + Graphene	PBO-T

FIGURE 3 Images of mixtures P and PBO nanofiber mats: a) before diesel oil sorption b) after diesel oil sorption [Color figure can be viewed at wileyonlinelibrary.com]

of the nanofibers fabricated from the five different solutions was carried out using a SM Zeiss LS-10 microscope with an accelerating voltage of 20 kV after the non-conductive samples had been coated with gold via electro-deposition. Three-dimensional (3D) AFM images and image profiles revealed the interchange in the topography of the electro-spun nanofibers. FTIR spectra analysis of the nanocomposite with PBO was conducted with a Bruker
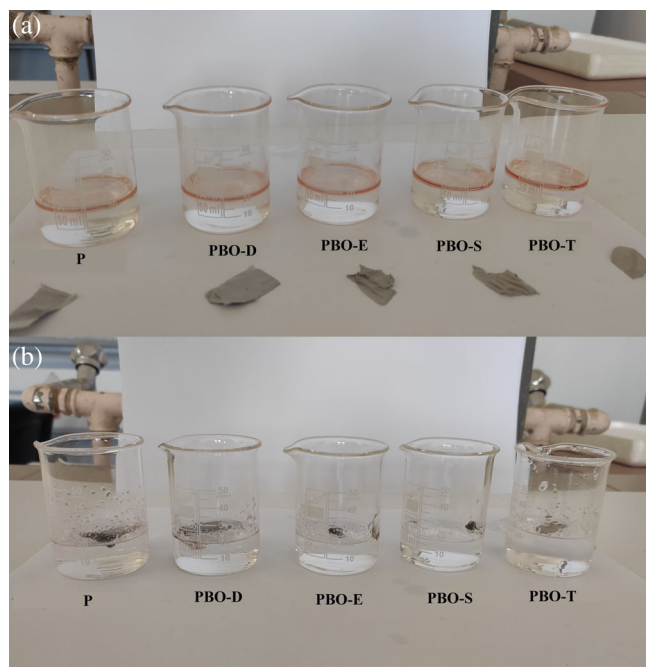
Vertex 70 in the range of 400 and 4000 cm^{-1}. TGA-DSC were conducted with a METTLER STAR SW thermal analyzer under an N2 atmosphere at a heating rate of 10 C/min from 25 °C to 900 °C. XRD analysis was conducted from 5° to 80° with a Bruker D8 X-ray diffractometer equipped with a Cu Kα anode (λ=1.541 Å)."

In this study, CA measurements were performed at five points on fiber mats using goniometer (Model OCA 50, DataPhysics Instruments GmbH, Filderstadt, Germany). The BET data were measured by Micromeritics tristar II plus 3020.

2.4 | Computational methods

The data were collected from 60 experiments of five different nanofiber mats, namely P, PBO-D, PBO-E, PBO-S, and PBO-T. We intended to evaluate the effect of the experimental conditions on the DOSC value. The main aim of the application was to determine an optimal combination of the experimental conditions (i.e., nanofiber mats, time t (1–4 min), and ratio of diesel oil to water (0.25, 0.5, and 0.75) that would maximize the DOSC value. Among the covariates, we also included the mass of the sorbent nanofiber after tap water sorption (g), that is, m_w. To conduct the computational study, we used the Caret,[68] Metrics,[69] and SHAPforxgboost[70] packages in the R.

2.4.1 | Random forest

RF, which was introduced by Breiman,[71] is a supervised machine learning model applicable for regression and classification problems. It is an ensemble model, g, which combines n number of decision trees, f, as follows

$$g(x_1,...,x_n) = \sum_{i=1}^{n} f_i(x_1,...,x_n). \qquad (2)$$

The output of the model is the aggregated result of all the independent decision trees trained on different samples by bootstrap aggregating. The ensemble model overcomes the overfitting problem, thereby resulting in high prediction accuracy.

2.4.2 | Extreme gradient boosting

Extreme gradient boosting (XGBoost) is a machine learning method relying on a tree boosting system that was proposed by Chen and Guestrin.[61] Scalability, high-speed performance, and good control against overfitting make the model applicable for highly unbalanced data.

The decision trees are built one at a time, and each new tree is improved considering the residuals from a previously trained tree.

One of the differences between XGBoost and RF is that the former performs optimization, which is to minimize a loss function, over the functional space. However, RF does not have a loss function, and optimization is performed over the parameter space.

2.4.3 | Performance metrics

To evaluate the prediction performances of the models, three most common metrics, namely, MAE, MAPE, and RMSE, were used. The formulas of the performance indicators are illustrated in Equations 3–5,

$$MAE = \frac{1}{n}\sum_{t=1}^{n} |P_t - E_t|, \qquad (3)$$

$$MAPE = \frac{1}{n}\left(\sum_{t=1}^{n} \frac{|P_t - E_t|}{|E_t|}\right) * 100, \qquad (4)$$

$$MAE = \sqrt{\frac{\sum_{t=1}^{n}(P_t - E_t)^2}{n}}, \qquad (5)$$

where P_t denotes the predicted value, E_t an experimental value, and n the number of experiments.

3 | RESULTS AND DISCUSSION

3.1 | Characterization of the nanofiber mats

The hybrid PVDF polymers used in the production of PBO nanofibers are one of the important materials used in energy harvesting application studies. Factors such as excellent chemical resistance, good strength, biocompatibility and low melting temperature as well as β phase formation make them one of the promising candidates for piezoelectric energy harvesting applications. Therefore, the increase and improvement of β phase are important for an efficient piezoelectric sensor. In this study, nanofiber was obtained by electrospinning method with low cost for the enhancement of the β phase of PVDF.[72,73] The phase of PVDF with the highest dipole moment 8×10^{-30} in the unit cell is specified as the "β phase".[74,75] By XRD, the β phase is seen in the crystal plane at $2\theta = 20.3°$ of the (110) reflections[76,77] and $2\theta = 36.2°$ of the (101) reflections.[78] The highest crystal peak

intensity was observed in PBO-E. By adding 0.3% graphene to the PVDF, the highest polar β phase was obtained.[77,79,80,81] An increase in the β phase peak intensity was observed upon PBO addition. According to their peak intensities shown in Figure 4(a), the order of the mats is as follows: PBO-E > PBO-D > PBO-T > PBO-S. The small peak before the main β phase peak is the α-phase and was observed at $2\theta = 18.4°$ of the (020) reflections.[76,80]

When the FTIR spectra of the nanofiber mats obtained within the range of 400 and 4000 cm^{-1} is examined, characteristic β phase FTIR peaks are observed at 510,[76,82] 598,[76] 840,[77,83,84] and 1400 cm^{-1}.[85] The β phase in the nanofiber mat increases with the width of these peaks. From Figure 4(b), it is evident that the peak widths between 840 and 598 cm^{-1} are ordered as follows: PBO-E > PBO-D > PBO-T > PBO-S > P.

According to Figure 4(c), the first decomposition temperature values of nanofiber mats were obtained to be 10–30°C higher than that of pure PVDF. The first

decomposition temperatures were determined as follows: PBO-D: 480°C, PBO-S: 472°C, PBO-T: 470°C, and PBO-E: 475°C. There are two explanations for the increase in the thermal resistance. First, the β phase of PVDF was completely trans structured, and the trans chains were tightly intertwined with graphene. Second, the thermal resistance of PBO is high.[86]

The percentage of the substance contents in the nanofiber mat was calculated by TGA analysis. The thermal decomposition of P occurred at between 300 and 520°C.[87] In the fabricated PVDF/PBO/graphene nanoparticles (i.e., PBO-T, PBO-D, PBO-E, and PBO-S), PVDF decomposition occurred at between 300 and 520°C, and PBO decomposition occurred at temperatures higher than 550°C. Therefore, the fraction of nanofiber mats and PVDF could be calculated using mass loss in the temperature range of 300–520°C. The percent weight loss is calculated by Equation 6 for the 300–500°C range.[88] As evident from Table 2, the mass percentage of PVDF was the highest for PBO-S.
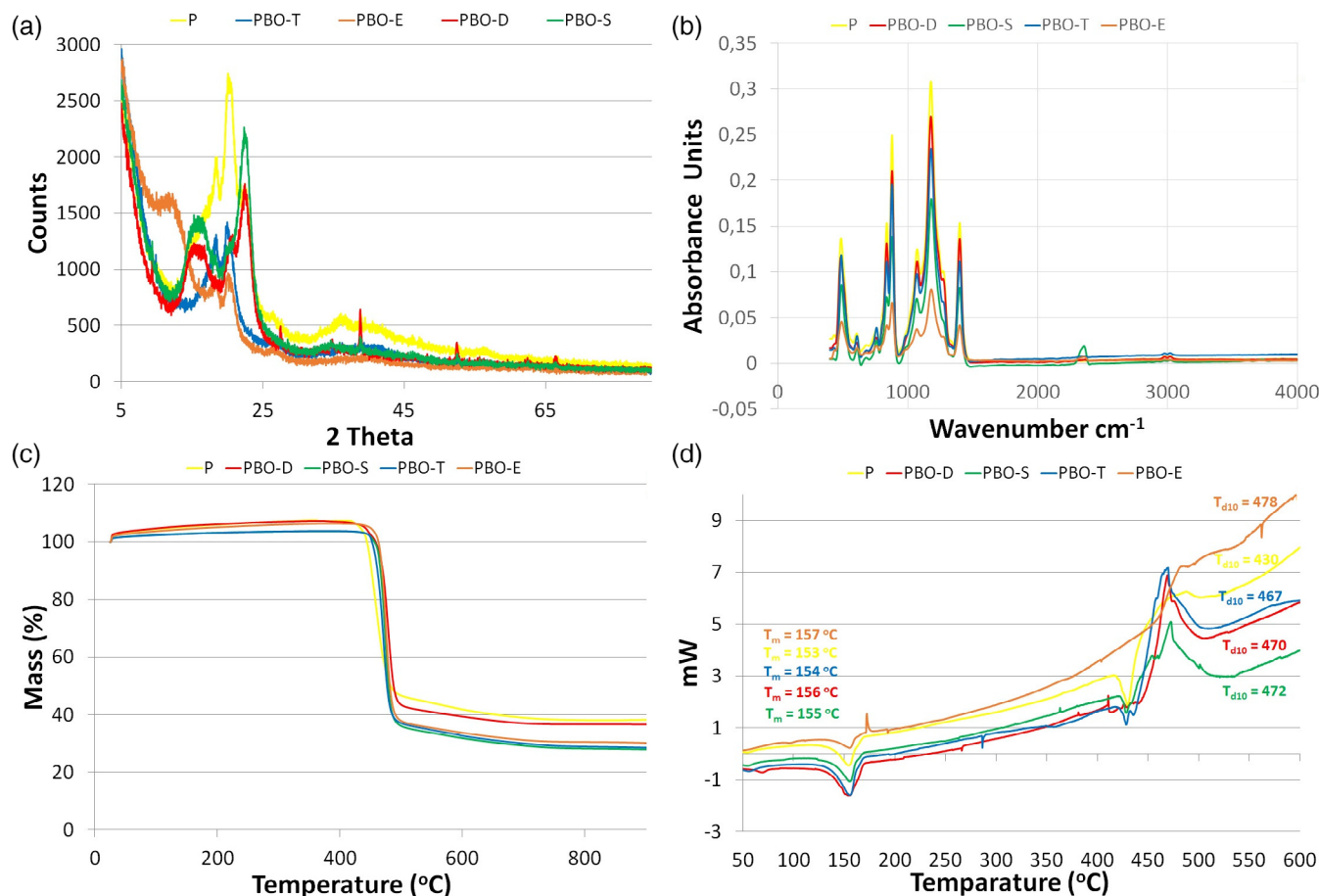
FIGURE 4 (a) XRD (b) FTIR spectra (c) TGA (d) DSC analysis of the composite nanofiber mats. DSC, differential scanning calorimetry; FTIR, Fourier transform infrared spectroscopy; TGA, thermal gravimetric analysis; XRD, x-ray diffraction [Color figure can be viewed at wileyonlinelibrary.com]

TABLE 2 The PVDF fraction calculated from mass loss and PBO content percentages for the nanofiber mats between 300 and 520°C, T_m and T_{d10} values, mass percentage content based on EDX analysis, average roughness and RMS values

Composite nanofiber mats	Mass percentages in composite nanofiber mats	TGA results (°C)		Mass percentage content of the nanofiber mats (wt%)		AFM results (nm)		
		T_m	T_{d10}	F	C	Oth.	RMA	RMS
P	Graphene = 35 PVDF = 65	153	-	70.19	29.35	0.46	290.44	371.81
PBO-D	PBO-D/ Graphene = 35 PVDF = 65	156	470	72.42	27.28	0.30	258.90	316.86
PBO-S	PBO-S/ Graphene = 30 PVDF = 70	157	478	74.92	24.91	0.17	301.53	400.34
PBO-T	PBO-T/ Graphene = 29 PVDF = 71	155	472	77.75	21.96	0.29	236.23	313.13
PBO-E	PBO-E/ Graphene = 30 PVDF = 70	154	467	74.86	24.80	0.34	285.72	388.36

$$PVDF\% = \frac{\text{Fiber decomposition} - \text{PBO}\% \text{ decomposition}}{0.92 - \text{PBO}\% \text{ decomposition}}.$$

(6)

In this study, the melting temperatures of the nanofiber mats were observed as an endothermic peak in the range of 150–157°C for the β phase, as shown in Figure 4(d).[78,83] T_m was observed to be 153°C for P (without the PBO additive). The T_m value increased upon PBO addition. When the endothermic decomposition peak for PVDF was examined, the PVDF decomposition temperature (T_d) was observed to be 430°C for PVDF/graphene. Endothermic decomposition peaks were not observed for PBO-T, PBO-D, PBO-E, and PBO-S nanofiber mats upon addition of PBO. T_{d10} produced a mass loss of 10%, as a result of PBO decomposition in the nanofiber mats, and the T_{d10} value was in the range of 460–470°C for the PBO doped nanofiber mats.

The surface properties of the nanofiber mats before diesel oil sorption were analyzed by SEM, AFM, CA measurements and BET analyses. The SEM images of the PBO nanofiber mats and fiber diameter distribution are shown in Figure 5.

The distribution of the fiber diameter of all the mats is substantially different. For P, approximately 90% of the fibers had 40–90 nm diameter width, and approximately 10% of the fibers had 110 nm diameter widths. Additionally, 60% of the P fibers, which had a homogeneous diameter width, had 60 nm widths, and 6% of the P fibers had above 100 nm diameter width. The PBO-D fibers had a diameter distribution between 60 and 130 nm, and 25% of the fibers had 70 nm width, 17% had 80 nm width, and 36% had 100 nm and above width. Moreover, the PBO-D fibers had a linear and beadless structure. 98% of the PBO-S fibers had a diameter width in the range of 40–90 nm, and 2% had diameter width of 100 nm. Furthermore, 34% of the PBO-S fibers were 50 nm wide, and 32% of the fibers were 60 nm wide. The PBO-T fibers had a diameter distribution in the range of 50–140 nm. Notably, 20% of the PBO-T fibers had 90 nm diameter widths, 18% had 100 nm diameter widths, and 24% had 110–150 nm diameter width. The PBO-T fibers showed a beaded structure. Notably, 68% of the PBO-E fibers had diameter width below 100 nm. The diameter widths of most PBO-E, PBO-S, and P fibers were below 100 nm. This may be attributed to the strengthening of the intermolecular bonds owing to the hydrogen bridge in fibers. A small fiber diameter results in a small pore size and high oil absorption capacity.[89]

AFM analysis was performed to obtain information about the surface structures of the nanofiber mats. The AFM images are shown in Figure 6. For PBO-S and PBO-E, holes and prongs were not observed on the surface of the mats. However, P and PBO-D mats had prongs and deep slits. Upon adding PBO, the order of RMS and average roughness was as follows: PBO-T < PBO-D < P < PBO-E < PBO-S.

CA measurements of all PBO mats were carried out and angle changes over time graphs are given in Figure 7. According to the analysis, hydrophobic property in the air with a WCA value in the range of 132–140°. Overlapping nanofibers and randomly distributed air
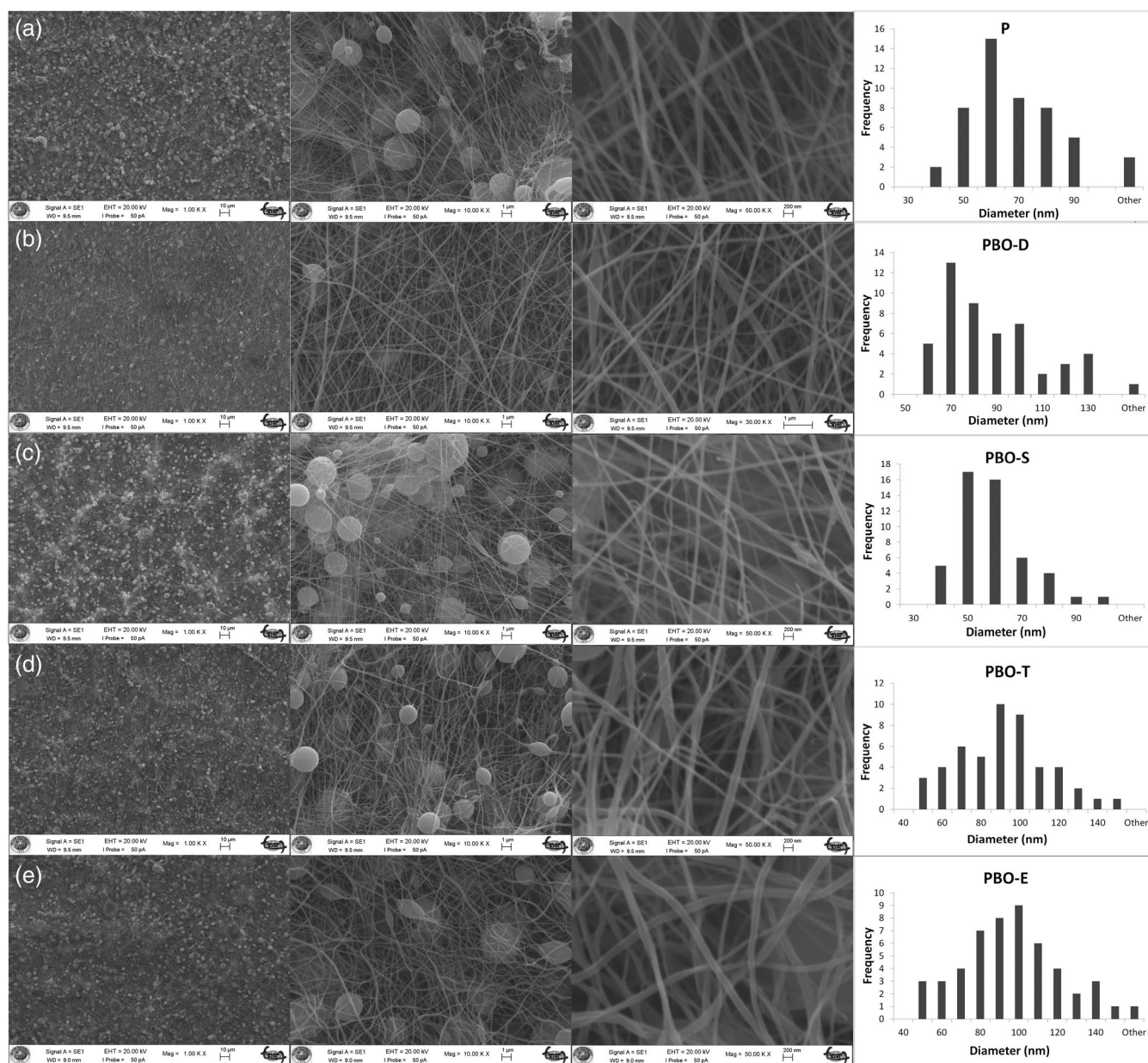
FIGURE 5 SEM images and fiber diameter distribution graph of composite nanofiber mats (a) P (b) PBO-D (c) PBO-S (d) PBO-T (e) PBO-E. SEM, scanning electron microscopy

pockets caused the CA to rise. The WCA change occurring in this range is due to the PBOs, which have different main chain structures in the content of the mats, as well as the surface roughness. In addition, WCA's of PBO-E and PBO-S were very close to each other as 139.8° and 140.0°. According to the WCA change graph over time, we can say that the fiber mats show stability. In the air, as soon as diesel oil contact the surface of the mat, oil spread rapidly on the mat surface and oil contact angle (OCA) was measured value in the range of 11.9°–17.3°. All mats showed superoleophilicity spread in the air. OCA values were measured in PBO-E and PBO-S as 11.9°

and 12.2°, respectively as the most oleophilic material and they are very close to each other. According to an OCA analysis in the air, it was observed that at the end of the 5th second, the oil on the surface was rapidly absorbed by the mat and the OCA values decreased. For PBO-E, an OCA value of less than 7° was obtained after 1.25 s. The smallest OCA value in the water environment was measured as 46.5° for PBO-E. P, PBO-T and PBO-S showed nearly the same OCA values in the water. The highest OCA value in the water was observed in PBO-D with 86.6°. According to an OCA analysis in the water, at the 3rd second, the OCA value of the PBO-E fiber mat
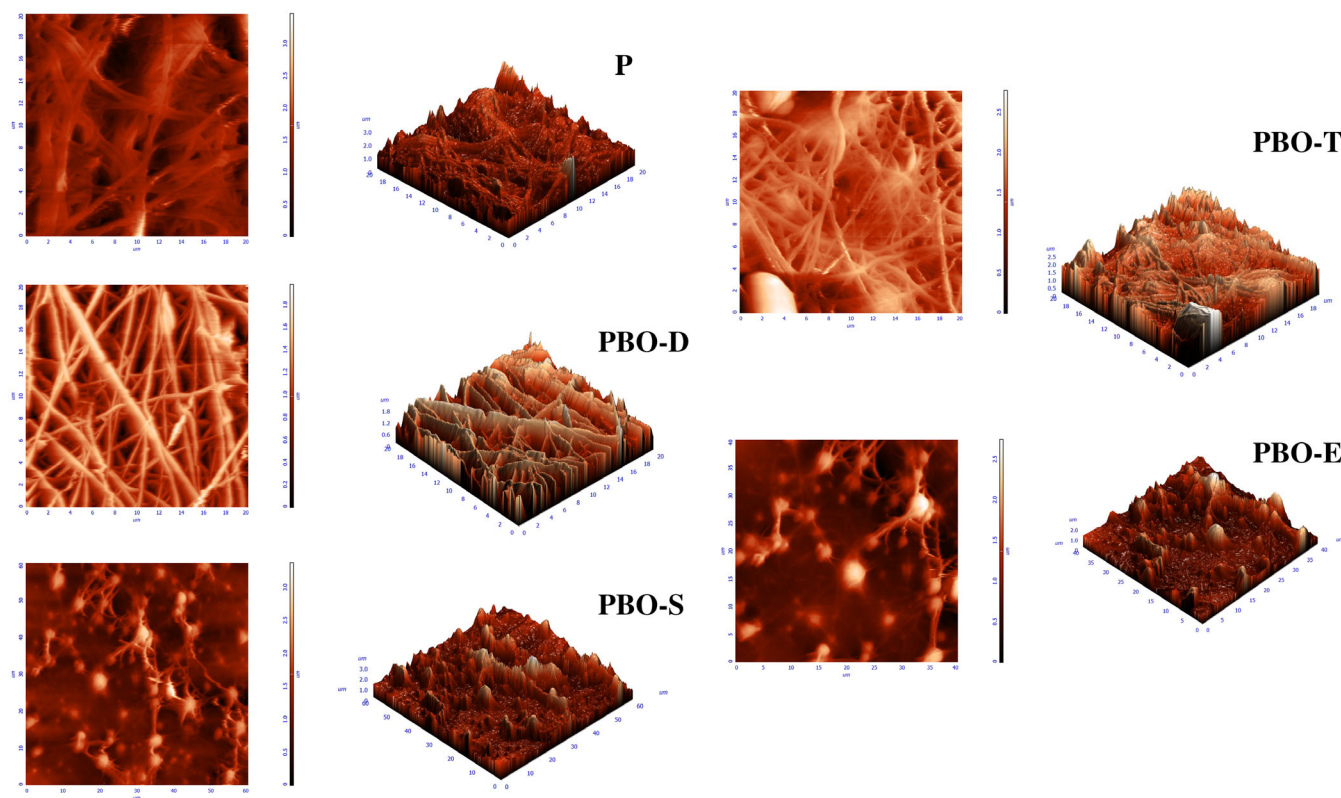
FIGURE 6 AFM images of composite nanofiber mats. AFM, atomic force microscopy [Color figure can be viewed at wileyonlinelibrary.com]

in the water has dropped below 10°. For PBO-S, after 2.5 s, the OCA value in the water dropped below 15°.

Nitrogen adsorption–desorption analyses were performed for all nanofiber mats to examine the surface area and pore structure. After the degassing process at 298 K for 10 h, N_2 adsorption–desorption isotherms were obtained at 77.3 K. The surface area of the materials was determined by the BET method, the pore volume and size were determined using the Barrett-JoynerHalende (BJH) method. Nitrogen adsorption porosimetry measurements were used to obtain information about the specific surface area and pore properties of the prepared PVDF electrospun nanofibers. Table 3 summarizes the specific surface area, pore volume, and average pore size of all nanofibers. In addition, in the classification with respect to the pore size of the materials made by IUPAC, it was determined that the nanofibers were in the class of mesoporous (2–50 nm) materials. A partial decrease in pore volume and pore size was observed for nanofiber materials containing PBO compared to P. The surface areas showed a significant increase in PBO-D and PBO-E compared to P, while the surface area of PBO-S increased slightly. For PBO-T, the surface area decreased slightly. For PBO-E and PBO-S, the increase in nanofiber diameter also supports the increase in the surface area. The

reason P, PBO-T, and PBO-S have low pore volumes is that PBO and graphene are surrounded by the matrix PVDF. This has contributed to a decline in the surface area and thus, resulted to a low specific surface area. According to the measured isotherms (Figure 8), P, PBO-T, and PBO-S correspond to the low levels of micropore and mesopore, along with relatively low specific surface areas as shown in Table 3.

3.2 | Evaluation of the nanofiber mats sorption capacity and separation performances

The DOSC values of the nanofiber mats in mixtures, which contained different ratios of diesel/water, were experimentally measured at the end of the 1st, 2nd, 3rd, and 4th minutes. The corresponding experimental results are presented in Table 4. The highest DOSC value was determined for P to be 14.7 at a 0.25 diesel/water ratio at end of the 1st minute. Nevertheless, the P nanofiber mat structure degraded at the end of the 3rd and 4th minutes, and the sorption capacity decreased. Likewise, upon increasing the proportion of diesel for the P nanofiber mat, the sorption capacity decreased significantly due to
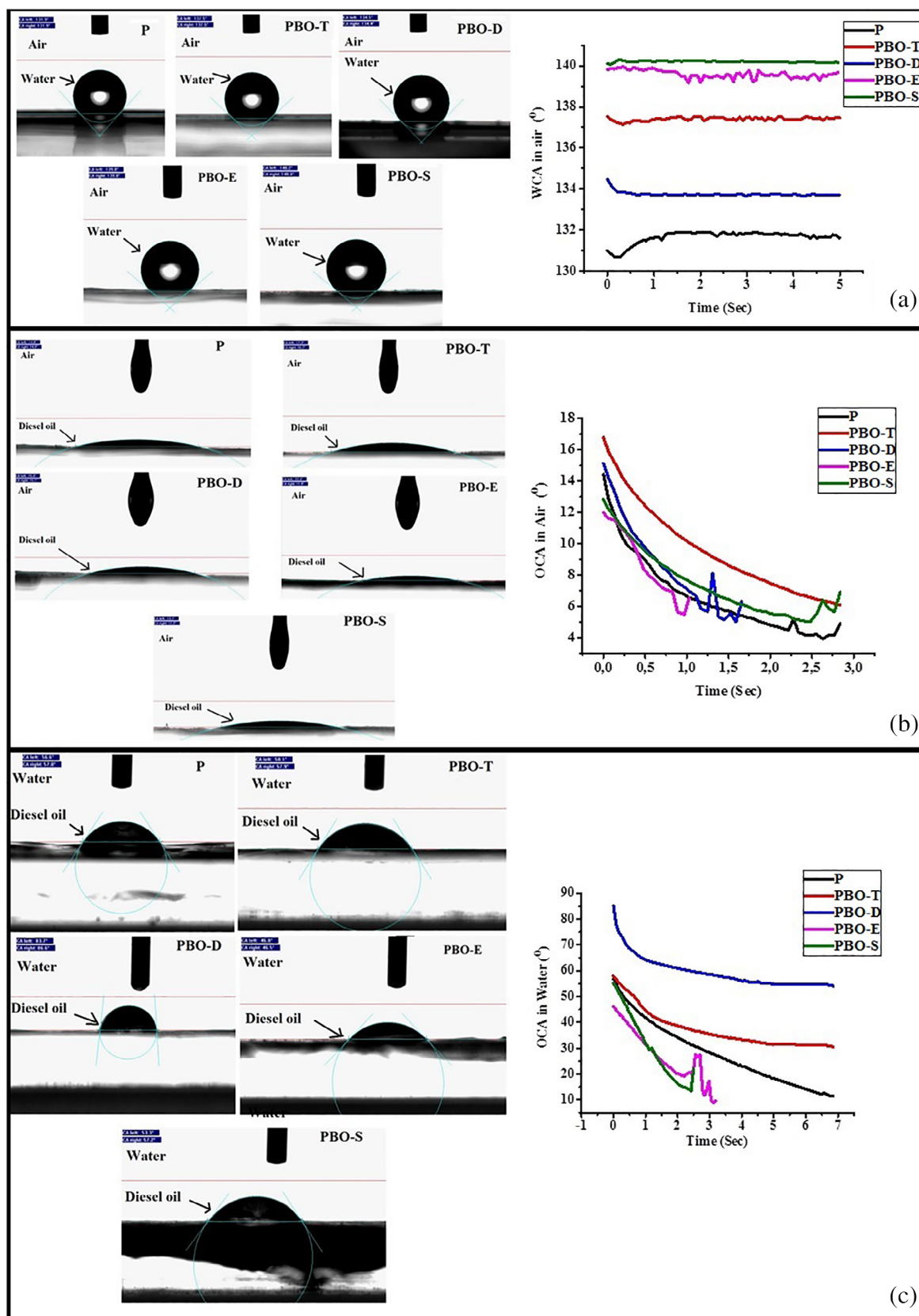
FIGURE 7 (a) WCA in the air b) OCA in the air c) OCA in the water. OCA, oil contact angle; WCA, water contact angle [Color figure can be viewed at wileyonlinelibrary.com]

SCIENCE

TABLE 3 Surface area, pore volume, pore size and CA measurements of nanofiber mats

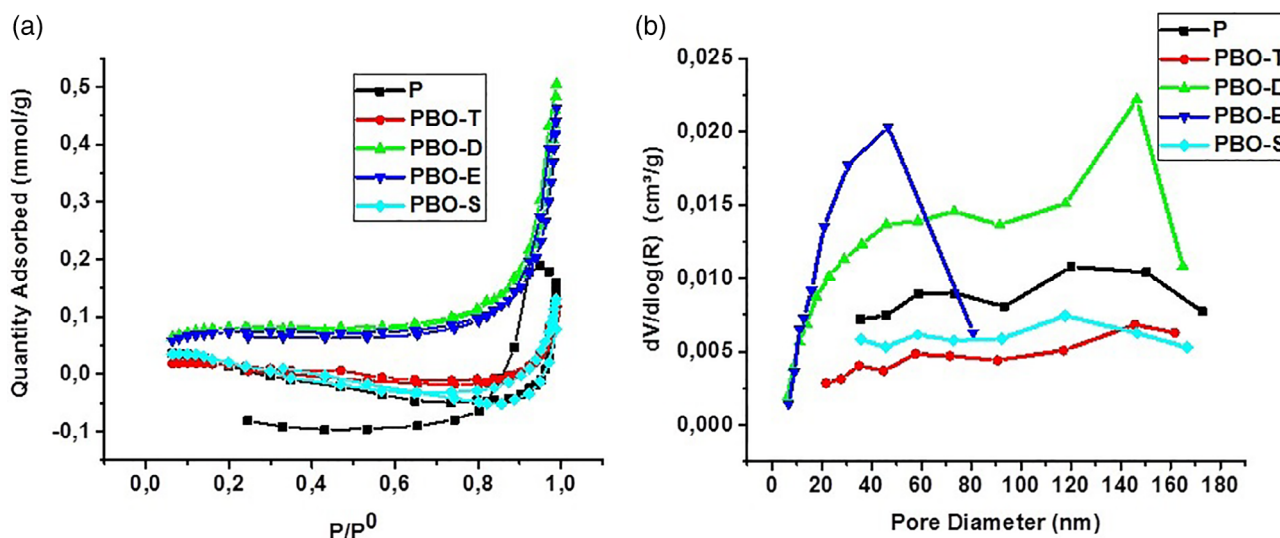| Nanofiber	Surface area (m^2/g)	Pore volume (cm^3/g)	Pore size (nm)	WCA	OCA	OCA in the water
P	1.31	0.0049	15.06	131.9	14.0	56.6
PBO-T	1.11	0.0032	11.55	137.5	16.2	57.9
PBO-D	6.56	0.0150	9.17	134.5	15.1	83.7
PBO-E	5.87	0.0136	9.27	139.8	11.9	46.5
PBO-S	1.66	0.0035	8.46	140.2	12.2	53.3

FIGURE 8 (a) Nitrogen adsorption–desorption isotherm of the nanofiber mats (b) pore size distribution curves of the nanofiber mats [Color figure can be viewed at wileyonlinelibrary.com]

TABLE 4 DOSC of the nanofiber mats in different volume ratios and minutes

	DOSC, VR:0				DOSC, VR:0.25			
	1st	2nd	3rd	4th	1st	2nd	3rd	4th
P	0.0013	0.0010	0.0007	0.0014	14.70	14.00	11.70	9.92
PBO-T	0.0017	0.0036	0.0024	0.0014	4.93	6.99	7.49	6.79
PBO-D	0.0011	0.0010	0.0011	0.0005	5.75	5.86	5.75	5.73
PBO-E	0.0006	0.0035	0.0036	0.0029	6.11	7.91	8.31	7.24
PBO-S	0.0027	0.0027	0.0015	0.0016	3.97	5.23	4.90	6.47
	DOSC, VR:0.5				DOSC, VR:0.75			
	1st	2nd	3rd	4th	1st	2nd	3rd	4th
P	5.42	6.05	6.23	6.42	5.58	5.92	5.86	4.85
PBO-T	8.71	8.47	9.24	10.32	6.24	6.72	7.04	8.00
PBO-D	8.46	7.43	6.41	5.68	6.05	6.16	5.89	5.63
PBO-E	12.94	10.14	10.86	9.33	6.20	6.92	7.78	5.67
PBO-S	5.87	7.20	8.91	10.09	5.95	7.40	7.57	7.04

the structure degradation. Upon adding PBO, the highest DOSC was determined to be 12.94 at a 0.5 diesel/water ratio at the end of the 1st minute for PBO-E. Although the sorption capacity decreased with time, no degradation was observed in the structure of the nanofiber mat at the end of the experimental period. The DOSC value increased with time, especially for the PBO-T nanofiber mat at a 0.75 diesel/water volume ratio. In this experimental study,

it was observed that the materials with PBO additive had a higher resistance to diesel than pure PVDF. PBO increased the chemical resistance of the material.

Figure 9 shows the images of water and diesel drops on the PBO-E nanofiber mat with the highest DOSC. It was observed that the diesel oil sorption occurred in a short time with high sorption capacity, and that the diesel oil was fully absorbed at the end of the 7th second. However the water drop was quickly taken up on the mat, and it was determined that the mat surface was not wet.

This study showed that the resistance of the material to solvents induced by PBO and graphene additives also helps the material to be recovered. The diesel oil absorbed by the nanofiber mats was kept in ethyl alcohol under room conditions, and afterward it was transitioned to alcohol in a very short time (Figure 10). The dry mass of PBO-T was initially taken as 0.0316 g and kept in a mixture of water and diesel oil at 9.5 mg/L concentration (0.2:20 ratio of oil and water with respect to the volume). The PBO-T mat kept in the oil/water mixture for 1 min absorbed the oil completely. PBO-T mat immersed in 20 ml ethyl alcohol and kept at room temperature without any mixing or pressure. The mat was separated from the filtrate and then the filtrate was taken to the evaporator and the 0.2 ml oil was separated from the filtrate. It was observed that the diesel oil significantly passed into the alcohol phase. The weight of the nanofiber mat removed from the alcohol was
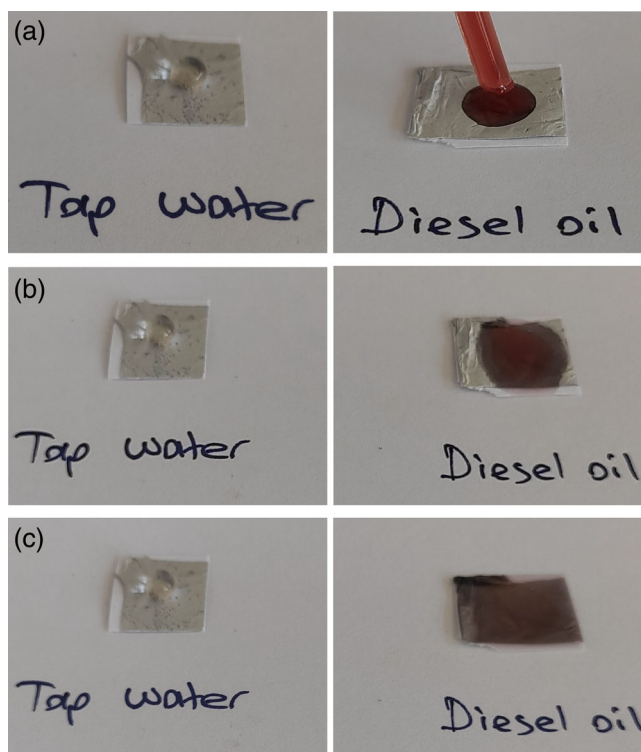
FIGURE 10 Time-dependent diesel oil and mains water retention comparison of PBO-T nanofiber mat: (a) 1st second (b) 3rd second (c) 7th second [Color figure can be viewed at wileyonlinelibrary.com]
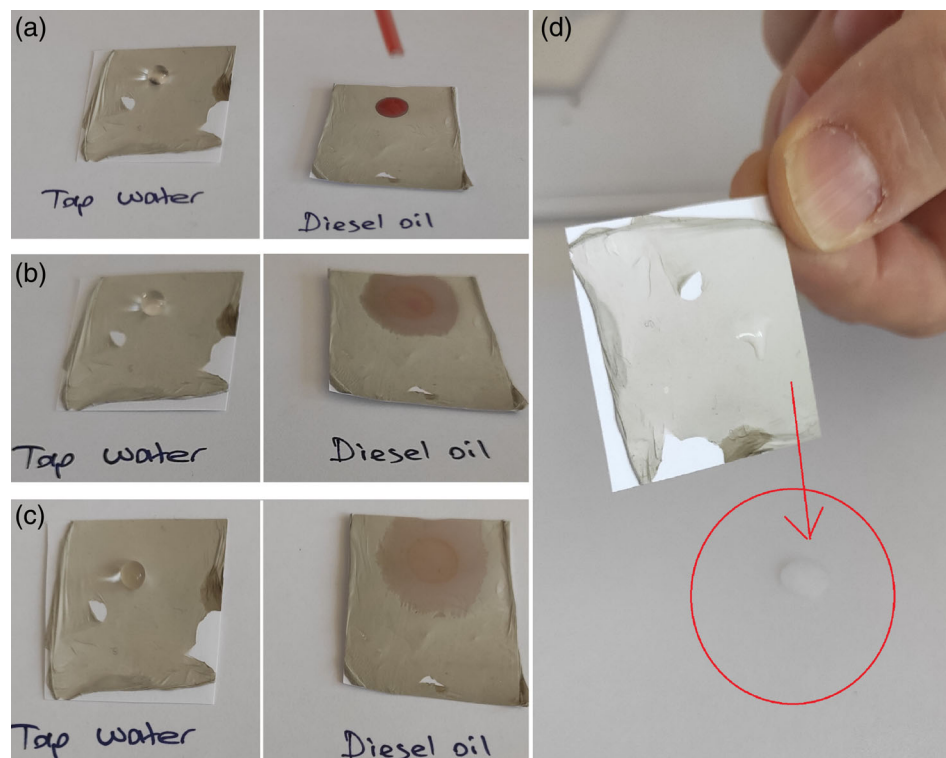
FIGURE 9 Time-dependent diesel oil and tap water retention comparison of PBO-E: (a) 1st second (b) 3rd second (c) 7th second (d) water droplet taken from the fiber surface after the 7th second [Color figure can be viewed at wileyonlinelibrary.com]

measured to be 0.0316 g. The diesel oil was taken into the alcohol phase without any damage to the structure of the nanofiber mat. The recovery process of the retained diesel oil in ethyl alcohol is shown in Figure 11. In this case, it has been shown that diesel oil can be recycled by distillation, and thus, the nanofiber mat can be reused.

The hydrophobic stability of the 1 cm^2 mats was examined against 10 ml of water. The water permeability of the mat was tested with the aid of blue-dyed water, which is only under the influence of gravity of 2 h in total (Figure 12(a)). The height of 10 ml of water added to the top part was taken as h = 10 cm. The intrusion pressure applied to the mat surface under the influence of gravity was calculated by Equation 7.[23] There was no water permeability in the mats at pressures below 10 kPa. At the end of 2 h, the highest water resistance (water rejection) was determined as 96% for PBO-E and PBO-S. Water resistance was determined as 93%, 92%, and 88% for PBO-D, PBO-T, and P, respectively. The graph of the water-resistance data at the end of 2 h is given in Figure 12(c).

$$P = \rho g h_{max}, \tag{7}$$

where g is a gravitational constant, h_{max} is a maximum height of water, and ρ is a water density.

The diesel oil permeability of the mats was tested by applying 10 ml of diesel oil from the top part of a glass tube. In 10 ml of diesel oil passed through all mats and diesel oil stored in the beaker in 30 min. Oil permeability of the nanofiber mats was determined as 98% and above.

To observe the behavior of P, PBO-T, PBO-D, PBO-E and PBO-S mats against a total mixture of 20 ml of diesel oil and water at a volume ratio of 1:1, 1 cm^2 mats were placed between the glass pipes in the setup given in Figure 12(b). The mixture was poured from the top of the glass tube. The volume of liquid passed through the membrane was measured. Owing to the hydrophobicity of the membranes and the underwater oleophobicity, the nanofiber mat has become a buffer between water and diesel oil. The water passed through the mat to the beaker below very easily. After 1 h, diesel oil was not found in the liquid part separated into the beaker. The separation efficiency of the P, PBO-T, PBO-D, PBO-E, and PBO-S mats after 1 h was calculated as 89%, 94%, 95%, 97%, and 96%, respectively (Figure 12(d)).

In addition, the slowly poured diesel oil and water mixture (V/V 1:1 ratio) from the top of the glass tube onto the nanofiber mats placed in the set-up was held for 1 h. The water permeated through the mat and was

Dry Fiber Mass

Diesel Oil Water Mixture

Diesel Oil Sorption

C$_2$H$_5$OH

Dried Fiber Mass After Diesel Oil Desorption
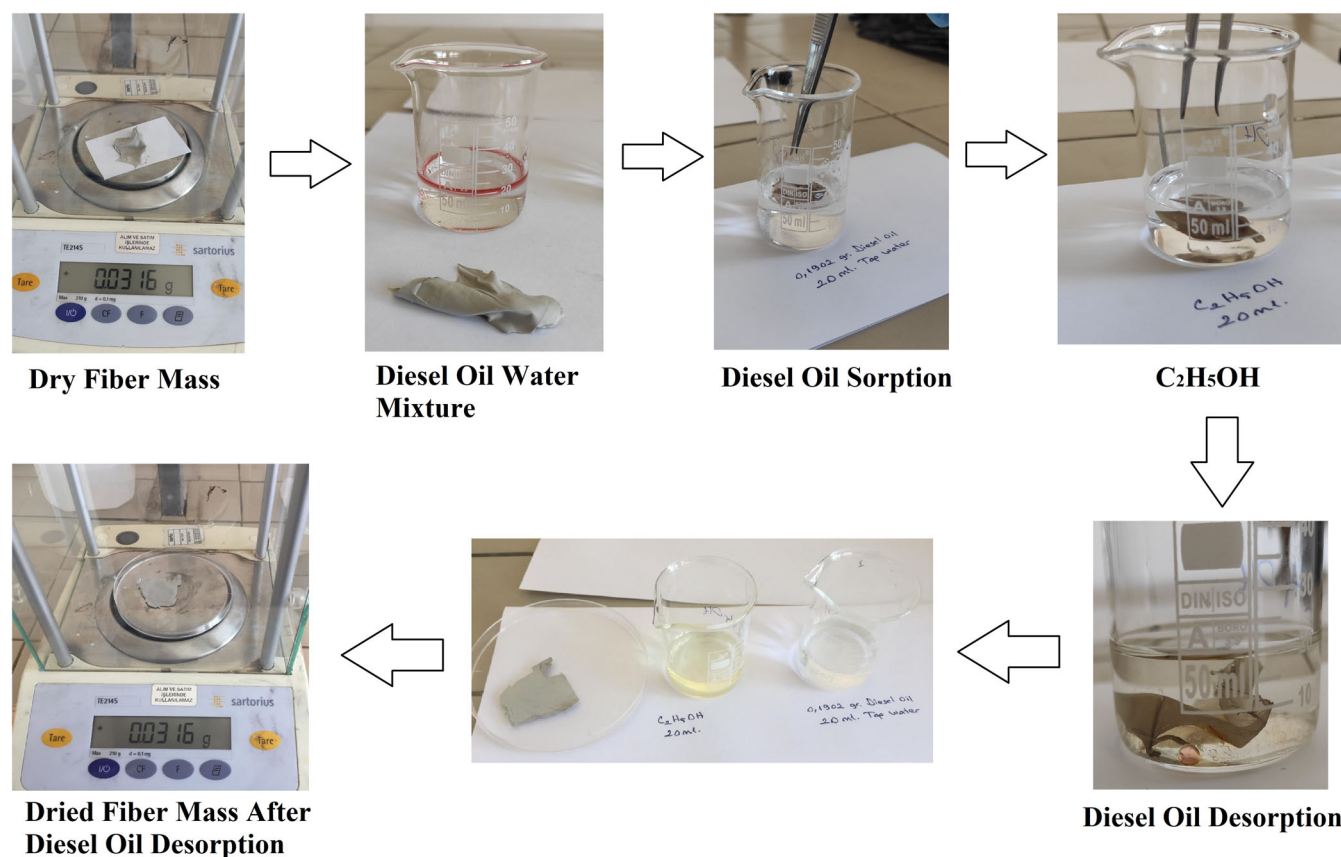
Diesel Oil Desorption

FIGURE 11 Recovery of retained diesel oil in ethyl alcohol [Color figure can be viewed at wileyonlinelibrary.com]
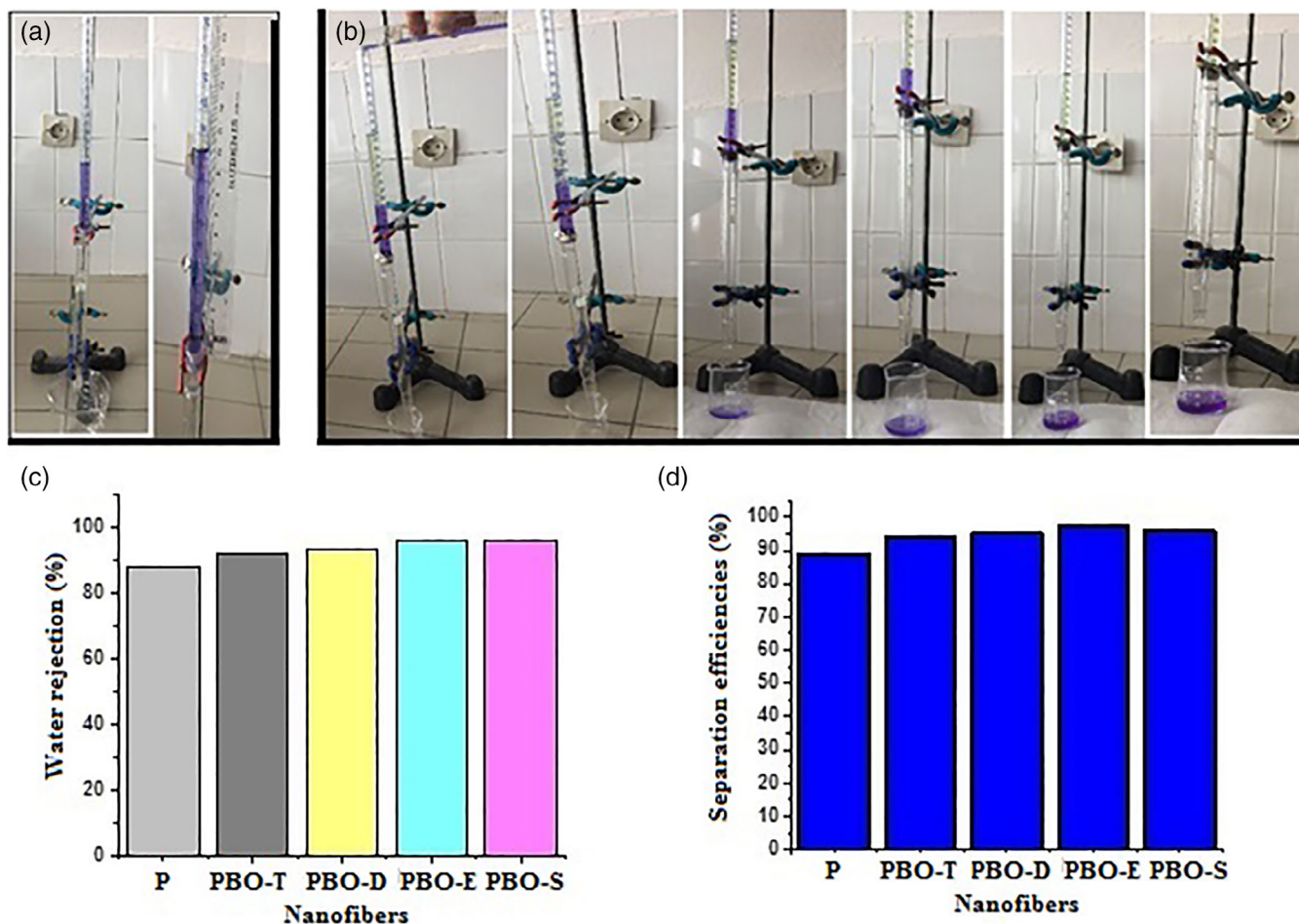
FIGURE 12 (a) the water intrusion (water is dyed with methyl blue) (b) diesel oil and water separation images of fiber mats (c) water rejection performance (d) separation efficiencies of the nanofiber mats [Color figure can be viewed at wileyonlinelibrary.com]

stored in the beaker. Volumetric flux of fluid is calculated by Equation 8,[23] and the flow graph of nanofibers is shown in Figure 13. The lowest flux value is observed for PBO-E at 1.1 Lm^{-2}h^{-1}.

$$Flux = V/(S \times t), \tag{8}$$

where V is the volume of permeating liquid, S is the effective area of the fiber mat, and t is the permeating time.

3.3 | Statistical and prediction analysis

Table 5 presents the descriptive statistics of the DOSC values of the five nanofiber mats. P has the highest DOSC value among all the other nanofiber mats; however, the variance of the DOSC value is high, considering the instability of the result. PBO-E has the highest mean and median value of the DOSC value and a relatively small variance. Despite PBO-E having the second-highest
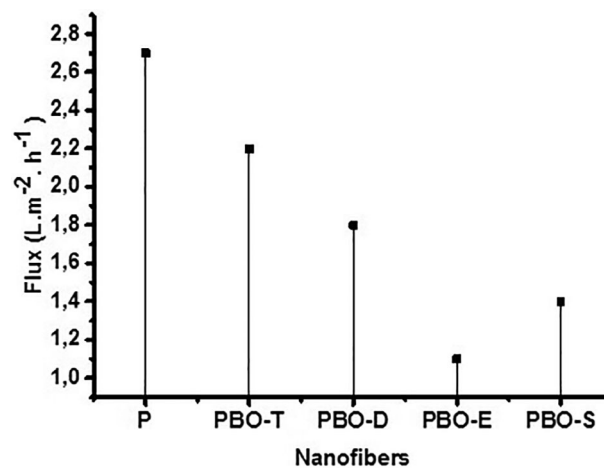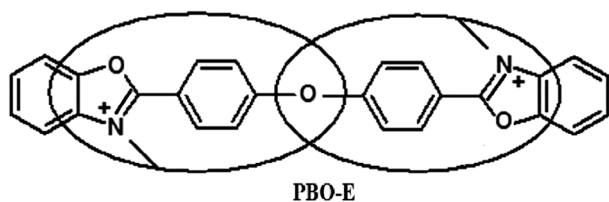

FIGURE 13 Result of the different nanofiber mats fluxes

DOSC, that is, 12.94, the descriptive statistics show that these results are stable and reliable, while P requires additional experiments to check the validity of the

WILEY *JOURNAL OF* **Applied Polymer** SCIENCE

TABLE 5 Descriptive statistics of the DOSC for five nanofiber mats

	P	PBO-D	PBO-E	PBO-S	PBO-T
Minimum	4.85	5.63	5.67	3.97	4.93
Mean	8.05	6.23	**8.28**	6.72	7.58
Median	6.14	5.88	**7.85**	6.76	7.27
Maximum	**14.70**	8.46	12.94	10.09	10.32
Variance	12.60	0.86	4.74	2.92	2.12

Note: Significance of bold values provide clear and easy demonstration of the values.

TABLE 6 Prediction performance (RMSE, MAE, and MAPE) of RF and XGBoost for three and four covariates

	RMSE	MAE	MAPE
RF (all covariates)	1.60	1.17	0.17
XGBoost (all covariates)	1.71	1.19	0.17
RF (three covariates)	1.56	1.13	0.15
XGBoost (three covariates)	**1.36**	**0.98**	**0.13**

Note: Significance of bold values provide clear and easy demonstration of the values.

FIGURE 14 Two adjacent system images connected with oxygen in PBO-E resonance feature

results. The stable and reliable results of PBO-E may be ascribed to the fact that the presence of oxygen along the chain increases the resonance stability. This stability might be a result of the involvement of unshared oxygen electrons in the resonance. Again, because of the oxygen, the hydrogen bond interactions between polymer chains make the polymer more regular and support the crystal phase. This may increase the resistance of the polymer to diesel oil. For the resonance feature of PBO-E, there exist two adjacent oxygen-and oxygen-connected systems that are more resonant than phenylene (Figure 14).[74]

We applied the RF and XGBoost models for three numerical variables, namely, proportion, time, and m_w and categorical variable nanofiber mats. Furthermore, for comparison reasons, we excluded the m_w variable and applied the ensemble machine learning models using only three covariates. We repeatedly and randomly apportion the data into training and test sets, with an 70–30% split and calculated an average prediction performance of the models measured on testing set, that is, the arithmetic mean of the RMSE, MAPE, and MAE (Table 6). According to the results, XGBoost for 3 covariates with 500 rounds, maximum depth of 2, $\eta = 1$, $\gamma = 10$, and a subsample of 50% outperforms the RF for 3 and 4 covariates and XGBoost for 4 covariates. Despite the small size of the data set, generally, models show an acceptable prediction performance. Noticeably, exclusion of m_w from the covariates improves the performance of the models.

The XGBoost is a non-parametric model that does not require the data to follow a specific distribution, hence the model does not require any transformation of the data. However this advantage has an obstacle, prediction interval is not produced by the model. To calculate the prediction interval of DOSC we used an ordinal bootstrapping method repeated 500 times. Bootstrapping takes a set of random samples from the original sample with replacement and repeats a large number of times the sampling procedure. The standard errors of the predicted DOSCs are computed from the bootstrap samples and used to obtain a 95% prediction interval.

Figure 15 displays the DOSCs predicted by the selected XGBoost model and corresponding experimental values with 95% prediction interval. The prediction performance of the model is significant, most of the predicted values are close to the experimental values and within the prediction intervals.

The model outcomes support the descriptive statistics of the experimental data set. According to the prediction intervals represented in Table 7, PBO-E with proportion of 0.5 measured at the end of the 3rd minute resulted in the highest lower bound of the prediction interval, that is, with 95% of confidence the sorption capacity will be at least 9.39 g/g sorbent. The more consistent and reliable results of PBO-E are ascribed to the fact that it is not degraded by diesel oil and mains water. Despite P with the diesel-oil/tap-water ratio of 0.25 measured at the end of the 1st minute, had the highest experimental DOSC value, 14.70 g/g sorbent; however, its prediction interval is wider than for other experiments, meaning greater uncertainty in the result. The experimental DOSC values produced by P have a high variance, which indicates unstable results. The underlying reason is that PVDF in P content had a low resistance against organic solvents (ether, DMF, etc.). Therefore, it degrades easily. If the P nanofiber mat is kept in diesel oil, it degrades within 1 min. Therefore, the mass of the P nanofiber mat decreases rapidly after the 2nd, 3rd and 4th minutes.

XGBoost is a powerful model in terms of prediction; however, because of the complexity of the model
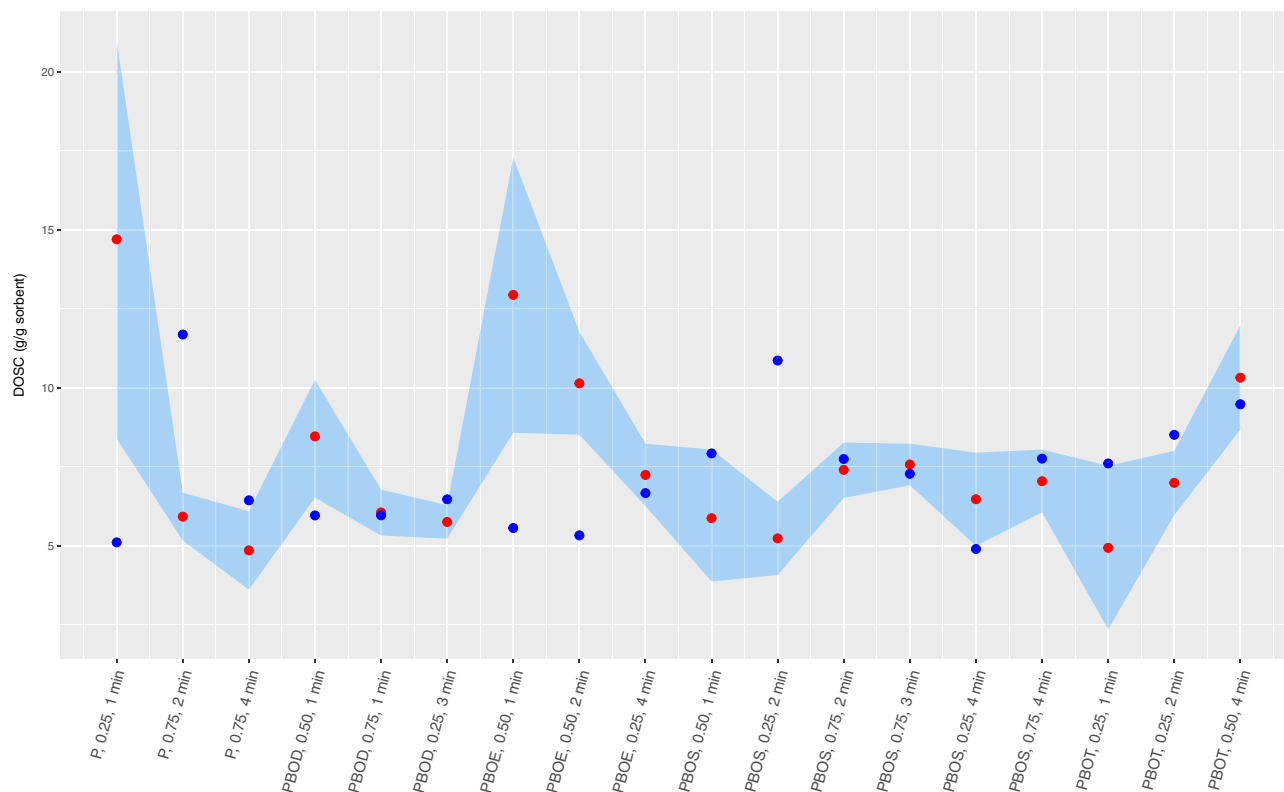
FIGURE 15 The experimental (red dots) and the predicted DOSC (blue dots) values for testing set. 95% prediction interval is displayed as a light blue shade [Color figure can be viewed at wileyonlinelibrary.com]

structure, it is difficult to analyze the background of the predicted results. To solve this problem, we used SHAP values to interpret the results of the selected model. SHAP is a method that allows any black-box model to be described as easily as a conventional regression model can be described. The power of SHAP values lie in their consistency and accuracy, thereby guaranteeing a confident interpretation of the model.

To accurately interpret the factors affecting DOSC values we factorize time and proportion variables and assume them as a categorical variable. Therefore, we apply XGBoost model with 500 rounds, maximum depth of eight, $\eta = 1$, $\gamma = 0$, and a subsample of 80% for three categorical variables, namely nanofiber mats, proportion and time. RMSE, MAE, and MAPE of the model are 1.02, 0.73, and 0.10, respectively.

Figure 16 includes SHAP values obtained from the model. The PBO-E mostly has a significant positive effect on the increase of DOSC value, meaning that on average PBO-E has a higher absorption capacity than the other nanofiber mats. The PBO-E surface morphology also supports this finding. The fiber diameter distribution obtained from the SEM analysis indicates that the PBO-E nanofiber mats mostly (68%) have a thinner fiber diameter. The thin fiber structure ensures that the surface roughness is higher and shows a highly

hydrophobic character. Therefore, DOSC is high for PBO-E. On the other hand, PBO-D and PBO-S have only a negative contribution to the DOSC value in comparison to the other nanofiber mats. The diameter width of the PBO-D nanofibers is greater than that of the PBO-E nanofibers. Additionally, the surface roughness of PBO-D is lower than that of PBO-E. PBO-S has the lowest fiber diameter and the highest surface roughness. However, because of the two sulfur atoms in the PBO-S main chain, its resistance to diesel oil is low. Therefore, diesel oil degrades PBO-S because of its sulfur content. Nonetheless, P has the highest significant positive effect on the response variable; however, the result is not consistent because it has also a significant negative effect on the DOSC value.

A diesel oil–tap water mixture with 0.5 ratio has the highest SHAP value, indicating that the ratio 0.5 is the most important feature affecting the DOSC. Furthermore, increasing the proportion of the diesel oil to 0.75 decreases the DOSC value and has a significant effect on the DOSC value. In summary, the proportion of 0.5 for any nanofiber mats and measured at any time results in higher DOSC value of an average of 0.8 g/g sorbent than the proportion of 0.25 and 0.75.

Experiments at the end of the 3rd minute witnessed a more positive and consistent trend regarding the DOSC

TABLE 7 The experimental DOSC with corresponding 95% prediction interval

Nano-fiber mats	Proportion	Time	Experimental DOSC	95% prediction interval
P	0.25	1	14.70	(8.39, 21.00)
P	0.50	1	5.42	(1.87, 8.99)
P	0.75	1	5.58	(4.00, 7.16)
P	0.25	2	14.00	(9.26, 18.74)
P	0.50	2	6.05	(3.91, 8.19)
P	0.75	2	5.92	(5.17, 6.67)
P	0.25	3	11.70	(8.76, 14.64)
P	0.50	3	6.23	(4.60, 7.86)
P	0.75	3	5.86	(5.11, 6.61)
P	0.25	4	9.92	(7.46, 12.38)
P	0.50	4	6.42	(5.00, 7.84)
P	0.75	4	4.85	(3.61, 6.09)
PBO-D	0.25	1	5.75	(4.23, 7.26)
PBO-D	0.50	1	8.46	(6.52, 10.25)
PBO-D	0.75	1	6.05	(5.32, 6.77)
PBO-D	0.25	2	5.86	(5.06, 6.67)
PBO-D	0.50	2	7.43	(6.39, 8.52)
PBO-D	0.75	2	6.16	(5.73, 6.57)
PBO-D	0.25	3	5.75	(5.22, 6.28)
PBO-D	0.50	3	6.41	(5.36, 7.54)
PBO-D	0.75	3	5.89	(5.38, 6.44)
PBO-D	0.25	4	5.73	(5.14, 6.32)
PBO-D	0.50	4	5.68	(3.89, 7.47)
PBO-D	0.75	4	5.63	(4.96, 6.30)
PBO-E	0.25	1	6.11	(1.94, 10.29)
PBO-E	0.50	1	12.94	(8.57, 17.28)
PBO-E	0.75	1	6.20	(3.88, 8.52)
Nano-fiber mats	**Proportion**	**Time**	**Experimental DOSC**	**95% prediction interval**
PBO-E	0.25	2	7.91	(6.56, 9.26)
PBO-E	0.50	2	10.14	(8.51, 11.77)
PBO-E	0.75	2	6.92	(5.89, 7.95)
PBO-E	0.25	3	8.31	(7.18, 9.43)
PBO-E	0.50	3	10.86	(9.39, 12.33)
PBO-E	0.75	3	7.78	(6.36, 9.20)
PBO-E	0.25	4	7.24	(6.26, 8.23)
PBO-E	0.50	4	9.33	(8.00, 10.66)
PBO-E	0.75	4	5.67	(3.96, 7.39)
PBO-S	0.25	1	3.97	(2.22, 5.72)
PBO-S	0.50	1	5.87	(3.87, 8.04)
PBO-S	0.75	1	5.95	(5.15, 6.75)
PBO-S	0.25	2	5.23	(4.07, 6.39)
PBO-S	0.50	2	7.20	(5.78, 8.62)
PBO-S	0.75	2	7.40	(6.51, 8.26)

(Continues)

TABLE 7 (Continued)

Nano-fiber mats	Proportion	Time	Experimental DOSC	95% prediction interval
PBO-S	0.25	3	4.90	(3.11, 6.70)
PBO-S	0.50	3	8.91	(7.22, 10.47)
PBO-S	0.75	3	7.57	(6.91, 8.23)
PBO-S	0.25	4	6.47	(4.99, 7.94)
PBO-S	0.50	4	10.09	(7.85, 12.30)
PBO-S	0.75	4	7.04	(6.06, 8.04)
PBO-T	0.25	1	4.93	(2.35, 7.53)
PBO-T	0.50	1	8.71	(6.69, 10.69)
PBO-T	0.75	1	6.24	(5.60, 6.91)
PBO-T	0.25	2	6.99	(5.97, 8.00)
PBO-T	0.50	2	8.47	(7.64, 9.31)
PBO-T	0.75	2	6.72	(6.22, 7.21)
Nano-fiber mats	Proportion	Time	Experimental DOSC	95% prediction interval
PBO-T	0.25	3	7.49	(6.45, 8.52)
PBO-T	0.50	3	9.24	(8.31, 10.20)
PBO-T	0.75	3	7.04	(6.35, 7.72)
PBO-T	0.25	4	6.79	(5.52, 8.07)
PBO-T	0.50	4	10.32	(8.68, 11.98)
PBO-T	0.75	4	8.00	(6.58, 9.40)
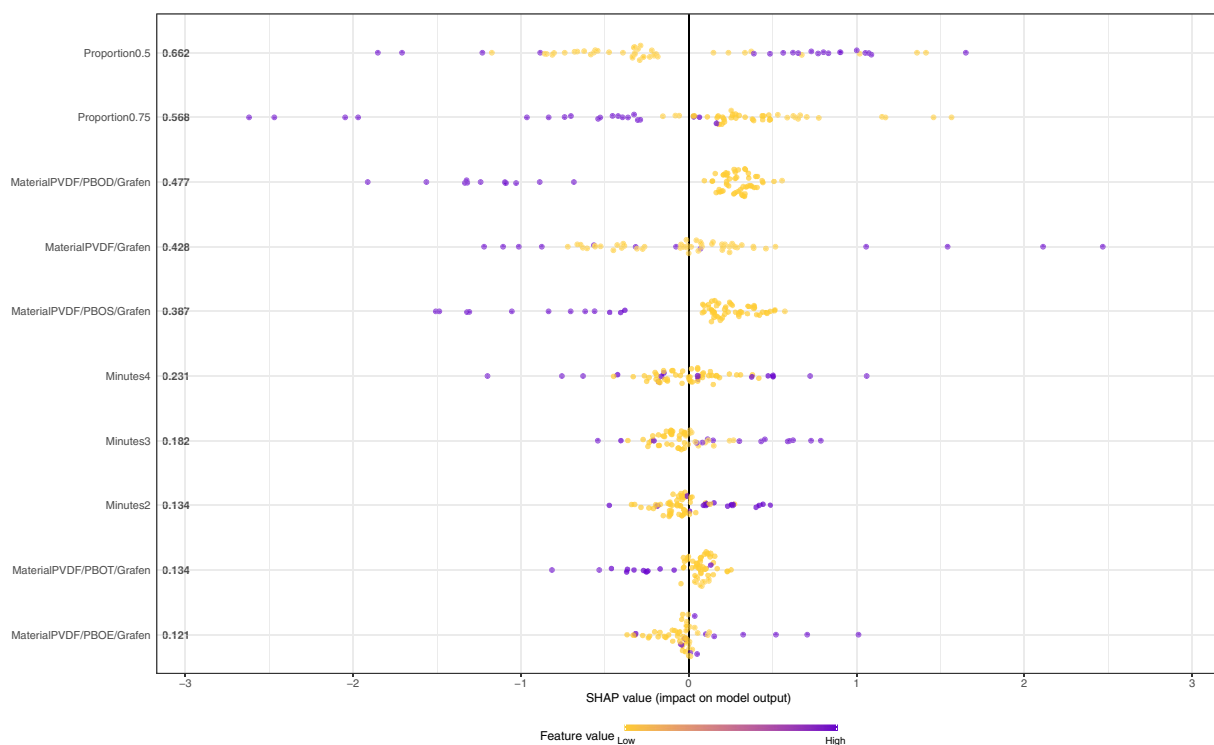
FIGURE 16 SHAP values for the XGBoost model. Significance of feature value impact is displayed by color varying from yellow (low impact) to violet (high impact). Zero SHAP value (vertical central line) indicates no impact of the feature. Positive feature impact is displayed by dots located on the right side of the vertical central line, negative feature impact is shown by dots on the left side of the vertical central line [Color figure can be viewed at wileyonlinelibrary.com]

value compared with the experiments at the end of the 1st, 2nd, and 4th minutes, implying that the measurements at the 3rd minutes resulted in higher DOSC value of an average of 0.25 g/g sorbent for any nanofiber mat and diesel-oil/tap-water ratio.

We suppose that the abovementioned findings might be useful for planning and conducting new experiments.

4 | CONCLUSIONS

In our study, we investigated the DOSC values of nanofiber mats containing four different solvent- and heat-resistant PBOs. The mats with homogeneous and linear fiber structures had an average diameter width in the range of 40–150 nm. The electrospun mats had DOSC in the range of 4.85–14.7 g diesel oil/g sorbent. According to the statistical analysis and XGBoost model, the PBO-E sorbent showed the most reliable and stable diesel oil sorption. PBO-E had a statistically consistent and high DOSC value at a 0.5 ratio of diesel-oil/tap-water measured at the 3rd minute with an experimental DOSC of 10.86 g/g sorbent. Moreover, according to XGBoost model, DOSC value for PBO-E is predicted to be at least 9.39 g/g sorbent and at most 12.33 g/g sorbent with 95% of confidence at a 0.5 ratio and the 3rd minute. Furthermore, the model explores that the proportion of 0.5 for any nanofiber mats measured at any time results in higher sorption capacity of an average of 0.8 g/g sorbent compared to the proportion of 0.25 and 0.75. The experiments measured at the end of the 3rd minute resulted in higher DOSC value of an average of 0.25 g/g sorbent compared with the experiments at the end of the 1st, 2nd, and 4th minutes for any nanofiber mats and any ratio of diesel-oil/tap-water. The explored optimal experimental settings might be helpful in preparing and performing new experiments.

The PBO nanofiber mats could be applied to eliminate oil and chemical leaks for industrial use on a wide scale. After the sorption of diesel oil, when the nanofiber mats were held in ethyl alcohol for a short time, the PBO nanofiber mats recovered their initial mass, and the diesel oil was transferred to the ethyl alcohol process. The followings are the recommendations for future studies:

- By conducting a diesel oil desorption study, the most usable PBO mats can be determined. The number of times the mats can be used and the desorption efficiency can be examined.
- The study can be extended by considering the antifouling property against various pollutants.
- Sorption and desorption studies of dyes which are among other important contaminants in water can be carried

out. By using porous and branched additives, fiber diameters can be reduced, higher porous mats can be obtained and higher sorption capacity can be achieved.

ORCID
Kamil Oflaz https://orcid.org/0000-0002-5345-3113
Zarina Oflaz https://orcid.org/0000-0003-3234-3879
Ilkay Ozaytekin https://orcid.org/0000-0002-0352-9458

REFERENCES
[1] A. Jernelöv, *Ambio* **2010**, *39*, 353.
[2] T. Arumugham, N. J. Kaleekkal, D. Rana, M. Doraiswamy, *J. Appl. Polym. Sci.* **2016**, *133*, 42848.
[3] T. T. Lim, X. Huang, *Chemosphere* **2007**, *66*, 955.
[4] S. Syed, *Environ. Pollut. Prot.* **2017**, *2*, 182.
[5] T. Zhang, G. S. Ellis, S. C. Ruppel, K. Milliken, R. Yang, *Org. Geochem.* **2012**, *47*, 120.
[6] P. J. Burgherr, *J. Hazard. Mater.* **2007**, *140*, 245.
[7] L. A. Soto, A. V. Botello, S. Licea-Durán, M. L. Lizárraga-Partida, A. Yáñez-Arancibia, *Front. Mar. Sci.* **2014**, *1*, 57.
[8] Y. Peng, Z. Guo, *J. Mater. Chem. A* **2016**, *4*, 15749.
[9] B. Mrayyan, M. N. Battikhi, *J. Hazard. Mater.* **2005**, *120*, 127.
[10] H. Wake, *Estuarine, Coastal Shelf Sci.* **2005**, *62*, 131.
[11] A. Chavan, S. Mukherji, *J. Hazard. Mater.* **2008**, *154*, 63.
[12] J. Beyer, H. C. Trannum, T. Bakke, P. V. Hodson, T. K. Collier, *Mar. Pollut. Bull.* **2016**, *110*, 28.
[13] E. J. Buskey, H. K. White, A. J. Esbaugh, *Oceanography* **2016**, *29*, 174.
[14] Y. Wei, Y. Jin, W. Zhang, *Int. J. Environ. Res. Public Health* **2020**, *17*, 1953.
[15] S. Jechalke, C. Vogt, N. Reiche, A. G. Franchini, H. Borsdorf, T. R. Neu, H. H. Richnow, *Water Res.* **2010**, *44*, 1785.
[16] O. T. Iorhemen, R. A. Hamza, J. H. Tay, *Membr. Water Treat.* **2017**, *8*, 395.
[17] T. Paulauskienė, I. Jucikė, N. Juščenko, D. Baziukė, *Water Air, Soil Pollut.* **2014**, *225*, 1959.
[18] S. M. Sidik, A. A. Jalil, S. Triwahyono, S. H. Adam, M. A. H. Satar, B. H. Hameed, *Chem. Eng. J.* **2012**, *203*, 9.
[19] L. Vlaev, P. Petkov, A. Dimitrov, S. Genieva, *J. Taiwan Inst. Chem. Eng.* **2011**, *42*, 957.
[20] V. Rajakovic, G. Aleksic, M. Radetic, L. Rajakovic, *J. Hazard. Mater.* **2007**, *143*, 494.
[21] S. Yang, M. Li, G. Fang, M. Xue, Y. Lu, *Colloids Surf., A* **2021**, *608*, 125611.
[22] J. Yong, J. Huo, F. Chen, Q. Yang, X. Hou, *Phys. Chem. Chem. Phys.* **2018**, *20*, 25140.
[23] X. Zhang, Y. Pan, J. Zhao, X. Hao, Y. Wang, D. W. Schubert, C. Liu, C. Shen, X. Liu, *Eng. Sci.* **2019**, *7*, 65.
[24] J. Cai, J. Tian, H. Gu, Z. Guo, *ES Mater. Manuf.* **2019**, *6*, 68.
[25] B. Yuan, L. Li, V. Murugadoss, S. Vupputuri, J. Wang, N. Alikhani, Z. Guo, *ES Food Agroforestry* **2020**, *1*, 41.
[26] L. Xie, O. Ciftci, Y. Zhang, *ES Food Agroforestry* **2020**, *1*, 77.
[27] J. L. Liu, X. Q. Feng, G. Wang, S. W. Yu, *J. Phys.: Condens. Matter.* **2007**, *19*, 356002.

[28] Z. Pan, F. Cheng, B. Zhao, *Polymer* **2017**, *9*, 725.

[29] C. Gao, W. Deng, F. Pan, X. Feng, Y. Li, *Eng. Sci.* **2020**, *9*, 35.

[30] P. Hou, R. Li, Q. Li, N. Lu, K. Wang, M. Liu, X. Cheng, S. Shah, *ES Mater. Manuf.* **2018**, *1*, 57.

[31] Y. Ma, Z. Zhuang, M. Ma, Y. Yang, W. Li, J. lin, M. Dong, S. Wu, T. Ding, Z. Guo, *Polymer* **2019**, *182*, 121808.

[32] Y. Ma, M. Ma, X. Yin, Q. Shao, N. Lu, Y. Feng, Y. Lu, E. K. Wujcik, X. Mai, C. Wang, Z. Guo, *Polymer* **2018**, *156*, 128.

[33] J. Chen, X. Wang, Y. Huang, S. Lv, X. Cao, J. Yun, D. Cao, *Eng. Sci.* **2018**, *5*, 30.

[34] J. Song, Y. Wang, J. Qiu, *ES Mater. Manuf.* **2018**, *3*, 29.

[35] D. Feng, S. Wang, Q. Zhuang, P. Guo, P. Wu, Z. Han, *J. Mol. Struct.* **2004**, *707*, 169.

[36] M. C. G. Jones, D. C. Martin, *Macromolecules* **1995**, *28*, 6161.

[37] D. C. Martin, E. L. Thomas, *Macromolecules* **1991**, *24*, 2450.

[38] S. Wang, P. Wu, Z. Han, *J. Mater. Sci.* **2004**, *39*, 2717.

[39] S. Wang, H. Lei, P. Guo, P. Wu, Z. Han, *Eur. Polym. J.* **2004**, *40*, 1163.

[40] B. Zhang, J. Yan, Z. Wang, *J. Phys. Chem. C* **2018**, *122*, 12831.

[41] V. Loianno, Q. Zhang, S. Luo, R. Guo, M. Galizia, *Macromolecules* **2019**, *52*, 4385.

[42] T. Woock, Master Thesis, University of North Dakota **2016**.

[43] P. Tsai, *Eng. Sci.* **2020**, *10*, 1.

[44] X. Lv, Y. Tang, Q. Tian, Y. Wang, T. Ding, *Compos. Sci. Technol.* **2020**, *200*, 108414.

[45] P. Yang, H. Zhao, Y. Yang, P. Zhao, X. Zhao, L. Yang, *ES Mater. Manuf.* **2020**, *7*, 34.

[46] L. Deng, H. Zhang, *ES Food Agroforestry* **2020**, *2*, 3.

[47] S. Angaiah, V. Murugadoss, S. Arunachalam, P. Panneerselvam, S. Krishnan, *Eng. Sci.* **2018**, *4*, 44.

[48] P. Panneerselvam, V. Murugadoss, V. Elayappan, N. Lu, Z. Guo, S. Angaiah, *ES Energy Environ.* **2018**, *1*, 99.

[49] V. Elayappan, V. Murugadoss, Z. Fei, P. J. Dyson, S. Angaiah, *Eng. Sci.* **2020**, *10*, 78.

[50] N. Sun, Z. Zhu, G. Zeng, *Sci. Total Environ.* **2020**, *744*, 140822.

[51] W. Zheng, J. Huang, S. Li, M. Ge, L. Teng, Z. Chen, Y. Lai, *ACS Appl. Mater. Interfaces* **2021**, *13*, 67.

[52] R. K. Gupta, G. J. Dunderdale, M. W. England, A. Hozumi, *J. Mater. Chem. A* **2017**, *5*, 16025.

[53] L. Kong, L. Ma, H. Jin, J. Hou, G. He, R. Zhang, *Polym. Adv. Technol.* **2019**, *30*, 1441.

[54] N. Aghajani, A. Gohari Ardabili, A. Daraei Garmakhany, *Iran. J. Nutr. Sci. Food Technol.* **2018**, *13*, 67.

[55] Z. Xu, L. L. Niu, M. Zhou, S. G. Zhang, *J. Gansu Agric. Univ.* **2015**, *25*, 2.

[56] E. A. Naghavi, R. Ghorbani, S. Bagherzadeh, *Iran. J. Food Sci. Technol.* **2018**, *14*, 134.

[57] A. Sadeghizadeh, F. Ebrahimi, M. Heydari, M. Tahmasebikohyani, F. Ebrahimi, A. Sadeghizadeh, *J. Environ. Manage.* **2019**, *232*, 342.

[58] H. Javadian, S. Asadollahpour, M. Ruiz, A. M. Sastre, M. Ghasemi, S. M. H. Asl, M. Masomi, *J. Taiwan Inst. Chem. Eng.* **2018**, *91*, 186.

[59] H. Javadian, M. Ghasemi, M. Ruiz, A. M. Sastre, S. M. H. Asl, M. Masomi, *Ultrason. Sonochem.* **2018**, *40*, 748.

[60] T. T. Nguyen, A. W. C. Liew, C. To, X. C. Pham, M. P. Nguyen, Paper presented at 13th International Conference on Machine Learning and Cybernetics, Lanzhou, **J2014**.

[61] T. Chen, C. Guestrin, paper presented at 22nd ACM SIGKDD International Conference on Knowledge Discovery and Data Mining, San Francisco, **2016**.

[62] S. M. Lundberg, S. I. Lee, *Adv. Neur. In.* **2017**, 4765.

[63] İ. Özaytekin, *Suleyman Demirel Univ. Fen Edebiyat Fak. Fen Derg.* **2007**, *2*, 188.

[64] İ. Özaytekin, Ph.D. Thesis, Selcuk University **2007**.

[65] İ. Özaytekin, İ. Karataş, *High Perform. Polym.* **2008**, *20*, 615.

[66] R. Barstugan, M. Barstugan, İ. Özaytekin, *Composites, Part B* **2019**, *158*, 141.

[67] Y. Yavuz, A. S. Koparal, Ü. B. Öğütveren, *Desalination* **2010**, *258*, 201.

[68] M. Kuhn, *J. Stat. Softw.* **2008**, *28*, 1.

[69] B. Hamner, M. Frasco, E. LeDell Package €˜Metrics€™ **2018**.

[70] Y. Liu, A. Just SHAPforxgboost: SHAP Plots for €™XGBoost €™, https://github.com/liuyanguu/SHAPforxgboost.html, **2020**.

[71] L. Breiman, *Mach. Learn.* **2001**, *45*, 5.

[72] G. Han, Y. Su, Y. Feng, N. Lu, *ES Mater. Manuf.* **2019**, *6*, 75.

[73] E. Ghafari, T. Nantung, N. Lu, *ES Mater. Manuf.* **2019**, *5*, 72.

[74] J. Gomes, J. Serrado Nunes, V. Sencadas, S. Lanceros-Mendez, *Smart Mater. Struct.* **2010**, *19*, 65010.

[75] P. Martins, A. C. Lopes, S. Lanceros-Mendez, *Prog. Polym. Sci.* **2014**, *39*, 683.

[76] A. Katoch, Ph.D. Thesis, Thapar University **2009**.

[77] J. Alamusi, L. Xue, N. Wu, J. Hu, C. Qiu, S. Chang, H. Atobe, T. Fukunaga, Y. Watanabe, H. Liu, J. Ning, Y. Li, Y. Li, Zhao, *Nanoscale* **2012**, *4*, 7250.

[78] A. Samadi, S. M. Hosseini, M. Mohseni, *Org. Electron.* **2018**, *59*, 149.

[79] A. Salimi, A. A. Yousefi, *Polym. Test.* **2003**, *22*, 699.

[80] M. El Achaby, F. Z. Arrakhiz, S. Vaudreuil, E. M. Essassi, A. Qaiss, *Appl. Surf. Sci.* **2012**, *258*, 7668.

[81] P. Han, J. Fan, M. Jing, L. Zhu, X. Shen, T. Pan, *J. Compos. Mater.* **2014**, *48*, 659.

[82] R. K. Layek, S. Samanta, D. P. Chatterjee, A. K. Nandi, *Polymer* **2010**, *51*, 5846.

[83] S. Lanceros-Méndez, J. F. Mano, A. M. Costa, V. H. Schmidt, *J. Macromol. Sci., Part B: Phys.* **2001**, *40*, 517.

[84] L. Yu, P. Cebe, *Polymer* **2009**, *50*, 2133.

[85] S. Satapathy, P. Gupta, S. S. Pawar, K. Varma arXiv.org, e-Print Arch., Condens. Matter **2008**.

[86] Y. G. Jeong, D. Baik, J. Jang, B. G. Min, K. H. Yoon, *Macromol. Res.* **2014**, *22*, 279.

[87] S. Shahgaldi, M. Ghasemi, W. R. W. Daud, Z. Yaakob, M. Sedighi, J. Alam, A. F. Ismail, *Fuel Process. Technol.* **2014**, *124*, 290.

[88] K. Yi, D. Geng, C. Shang, Y. He, J. Yang, Paper presented at 10th International Conference on Composite Science and Technology, Lisboa, **2015**.

[89] H. M. Choi, R. M. Cloud, *Environ. Sci. Technol.* **1992**, *26*, 772.